Objectively Analyzed Air–Sea Heat Fluxes for the Global Ice-Free Oceans (1981–2005)

BY LISAN YU AND ROBERT A. WELLER

Synthesizing surface meteorology obtained from satellite remote sensing and atmospheric model reanalyses leads to improved estimates of global latent and sensible heat fluxes.

The ocean and the atmosphere exchange heat at their interface via a number of processes—solar radiation, longwave radiation, sensible heat transfer by conduction and convection, and latent heat transfer by evaporation of sea surface water. The amount of heat being exchanged is called heat flux, and its distribution over the global oceans is required virtually for every aspect of climate studies (WGASF 2000). However, direct flux measurements are sparse. Our present knowledge of the global air–sea heat flux distribution stems primarily from the bulk parameterizations of air–sea fluxes as functions of surface meteorological variables (e.g., wind speed, temperature, humidity, cloud cover, etc.). The sources of observations for those flux-related variables include marine surface weather reports from voluntary observing ships (VOSs) collected by the Comprehensive Ocean–Atmosphere Data Set (COADS; Woodruff et al. 1998) and satellite remote sensing from various platforms. Atmospheric reanalyses from numerical weather prediction (NWP) centers such as National Centers for Environmental Prediction (NCEP) and the European Centre for Medium-Range Weather Forecasts (ECMWF) provide additional model-based databases. Nonetheless, none of these three data sources are perfect, because each suffers from at least one of the four following deficiencies: 1) incomplete global coverage, 2) relatively short time series, 3) systematic bias, and 4) random error.

The problems in data affect the accuracy of the resulting flux estimates. For instance, the COADS-based climatological flux atlases (Bunker 1976, 1980; Esbensen and Kushnir 1981; Isemer and Hasse 1985, 1987: Hsiung 1986; Oberhuber 1988; da Silva et al. 1994; Josey et al. 1998) were constructed from quasi-global ship observations that span several decades. The accuracy of these flux estimates depends on data-sampling density. In regions such as the tropical Indian Ocean and the southern oceans where VOSs are infrequent, the flux estimates have large uncertainties. The satellite-based flux products (e.g., Liu 1988; Chou et al. 1995; Schulz et al. 1997; Curry et al. 1999; Kubota

AFFILIATIONS: YU AND WELLER—Department of Physical Oceanography, Woods Hole Oceanographic Institution, Woods Hole, Massachusetts
CORRESPONDING AUTHOR: Dr. Lisan Yu, Dept. of Physical Oceanography, MS#21, Woods Hole Oceanographic Institution, Woods Hole, MA 02543
E-mail: lyu@whoi.edu

The abstract for this article can be found in this issue, following the table of contents.
DOI:10.1175/BAMS-88-4-527

In final form 5 January 2007

et al. 2002; Bentamy et al. 2003) are an attractive alternative, thanks to the continuous global coverage and good temporal and spatial resolution offered by remote sensing technology. However, satellite retrievals are not error free because they require ground truth for calibration and validation. They also have a relatively shorter record because most flux-related variables became available only after 1987. Furthermore, not all flux-related variables can be retrieved. Determining air humidity and temperature at a fixed level above the ocean surface remains a major technical challenge (Simonot and Gautier 1989; Schulz et al. 1993). By comparison, all flux-related variables are readily available from NCEP–NCAR reanalysis and 40-yr ECMWF Re-Analysis (ERA-40). Gridded global flux fields are provided at 6-h intervals from the 1950s onward. These NWP fluxes, unfortunately, contain systematic biases (e.g., Moyer and Weller 1997; Josey 2001; Smith et al. 2001; Sun et al. 2003). In some regions, such as the Arabian Sea (Weller et al. 1998) and the Bay of Bengal (Yu et al. 2007), the biases can be so large that the NWP net heat fluxes have a sign opposite to those of in situ flux measurements.

While improving the quality of each data source is a necessary step toward improving the estimates of surface heat fluxes, an alternative approach has been proposed. In a pilot study for the Atlantic Ocean supported by the National Oceanic and Atmospheric Administration (NOAA) Climate Variability and Predictability (CLIVAR) Atlantic program, Yu et al. (2004a) experimented with the idea of improving flux estimates through objectively synthesizing the satellite and NWP data sources. The term objective analysis (OA) originally denotes the process of combining data that are generally nonuniformly distributed and have errors associated with them. The process involves searching for a solution that has the minimum error variance (Daley 1991). Objective analysis has received wide application after its first introduction to the numerical weather prediction by Panofsky (1949), and now covers a broad range of techniques. The earlier ship-based flux climatological analyses (da Silva et al. 1994; Josey et al. 1999) used a simple iterative difference-correction scheme based on the method of successive corrections (Bergthorsson and Döös 1955). Modern OA techniques, such as statistical interpolation and variational analysis, have been applied to products such as sea surface temperature (SST) (Reynolds et al. 2002; Chelton and Wentz 2005), precipitation (Xie and Arkin 1996), pseudostress (Legler et al. 1989), and Special Sensor Microwave Imager (SSM/I) surface wind (Atlas et al. 1996). The OA technique explored by Yu et al. (2004a) was the variational approach similar to the one used by Legler et al. (1989).

The improvement in heat flux estimates made by the OA approach was evaluated by both statistical comparison and physical consistency study. The mean flux climatology from the OA analysis is in reasonable agreement with the ship-based flux climatology analysis of the National Oceanography Centre (NOC; named the NOC1.1 climatology; Josey et al. 1999) in data-dense regions, although the two were constructed from independent datasets using different techniques. The OA heat flux estimates differ from buoy–ship flux measurements by about 5% on average (Yu et al. 2004b, 2007). Comparison with the NWP fluxes is, however, not as good; they are 18–20 W m^{-2} (~15%) higher on average. An example that better fluxes can lead to a better understanding of SST variability was shown for the tropical Atlantic Ocean (Yu et al. 2006). Ocean observations indicate that the seasonal SST increase in the tropical Atlantic Ocean is associated with a shallow thermocline, suggesting that the major contributor to the surface mixed layer heat budget is the net surface heat flux through the air–sea interface (Niiler and Kraus 1977). By combining the OA latent and sensible heat fluxes with surface radiation from the International Satellite Cloud Climatology Project (ISCCP; Zhang et al. 2004), the role of surface heat fluxes was clearly depicted. As indicated by ocean subsurface observations, surface heat fluxes are the forcing for the seasonal SST cycle over most of the tropical Atlantic basin except for the equatorial cold tongue and the region under the intertropical convergence zone (ITCZ). Such a depiction cannot be established using NWP flux products from NCEP and ERA-40.

Motivated by the success made in the Atlantic basin, efforts have been undertaken to extend the OA to the heat flux fields over the global ice-free oceans under the auspices of the NOAA Office of Climate Observations (OCO) and Climate Change Data and Detection (CCDD). The goal of the Objectively Analyzed Air–Sea Fluxes (OAFlux) project is to develop an enhanced global analysis of air–sea latent heat, sensible heat, and net shortwave and net longwave radiation fluxes over the past 50 years (from the mid-1950s onward) through an appropriate combination of satellite retrievals, ship reports from COADs, and surface meteorology from NWP analysis/reanalysis outputs. The paper, which presents global daily air–sea latent and sensible heat fluxes for the period from 1 January 1981 to 31 December 2005, represents the first part of the results produced by the ongoing OAFlux project.

The paper has two main objectives—one is to provide an overview of the methodology used to produce the new global oceanic latent and sensible heat fluxes; and the other is to document the variability of ocean heat flux fields on annual, seasonal, interannual, and decadal time scales as revealed by the new dataset. Among all of the climate signals investigated in the study, the most striking is the pronounced long-term trend that dominates the 25-yr time series from 1981 to 2005. It is known that global oceans have been warming, and the majority of the warming has happened since the early 1980s (Levitus et al. 2000). The study provides evidence of the increase of oceanic latent heat losses in concert with the rise in SST. The paper concludes with a summary of the results and a discussion of potential applications of the dataset. For additional information on the OAFlux project and for access to the dataset, the reader is referred to the Web site at http://oaflux.whoi.edu/. [At that Web site, the reader also has access to the International Satellite Cloud Climatology Project (ISCCP) FD surface radiation dataset (Zhang et al. 2004), provided by Dr. William B. Rossow, for distribution along with the OAFlux products. The radiation data have been averaged daily and regridded so that both OAFlux and ISCCP products have the same spatial and temporal resolution.]

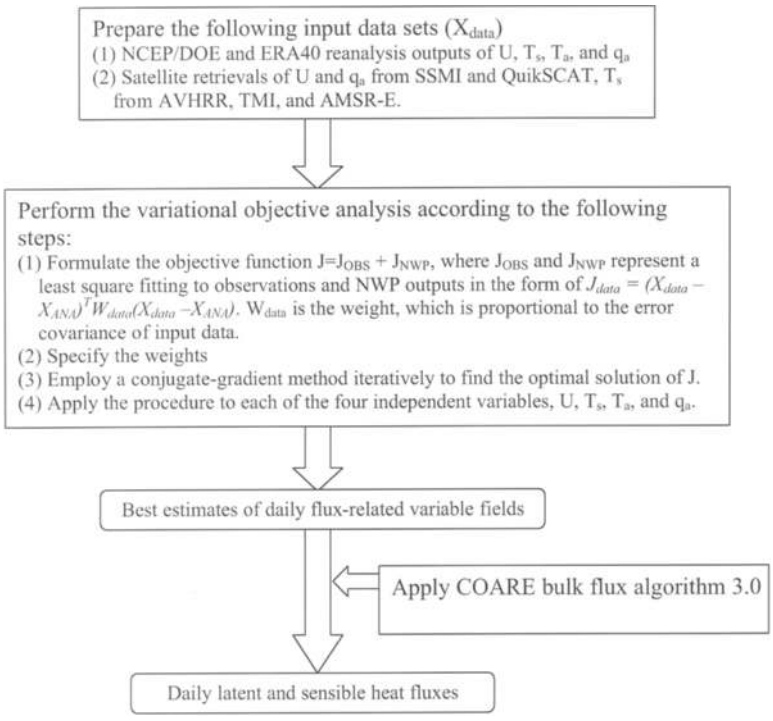

FIG. 1. A flowchart showing the procedure used in computing the latent and sensible heat fluxes through synthesizing surface meteorology from satellite retrievals and NWP reanalyses outputs.

METHODOLOGY AND INPUT DATA SOURCES. Surface latent heat flux (LHF) and sensible heat flux (SHF) are generally computed from the following bulk aerodynamic formulas (Liu et al. 1979):

$$\mathrm{LHF} = \rho L_e c_e U(q_s - q_a) = \rho L_e c_e U \Delta q, \quad (1)$$

$$\mathrm{SHF} = \rho c_p c_h U(T_s - T_a) = \rho c_p c_h U \Delta T, \quad (2)$$

where ρ is the density of air, L_e is the latent heat of evaporation, c_p is the specific heat capacity of air at constant pressure, c_e and c_h are the stability- and height-dependent turbulent exchange coefficients for latent and sensible heat, respectively, and U is the average value of the wind speed relative to the sea surface at a height of z_r; T_s and T_a are the respective sea surface and near-surface air potential temperatures, and the differences between T_s and T_a are denoted by ΔT; q_s and q_a are the respective sea surface and near-surface atmospheric specific humidities, and the differences between q_s and q_a are denoted by Δq. In (1)–(2), only U, T_s, T_a, and q_a are independent variables.

The key strategy implemented by the OAFlux project is to improve the estimates of LHF and SHF through improving the estimates of the four independent physical variables. This is achieved by using a variational OA technique to synthesize observations and NWP outputs. The methodology of synthesis is based on the Gauss–Markov theorem, a standard statistical estimation theory that states the following: when combining data in a linear fashion, the linear least squares estimator is the most efficient estimator (Daley 1991). In the case of our flux analysis, the theorem led to the formulation of a least squares problem based on available satellite retrievals and NWP model outputs. A solution that best fits the input datasets was searched. The procedure was applied to each of four independent variables (i.e., U, T_s, T_a, and q_a) from which the fluxes were computed using the bulk flux algorithm 3.0 developed from the Tropical Ocean Global Atmosphere (TOGA) Coupled Ocean–Atmosphere Response Experiment (COARE; Fairall et al. 1996, 2003). A flowchart showing the sequence of the procedure is given in Fig. 1. The

reader is referred to the paper by Yu et al. (2004a) for further information.

Input data for the synthesis included not only satellite retrievals from SSM/I (Wentz 1997; Chou et al. 2003), the Quick Scatterometer (QuikSCAT), Advanced Very High Resolution Radiometer (AVHRR), Tropical Rainfall Measuring Mission (TRMM) Microwave Imager (TMI), and Advanced Microwave Scanning Radiometer Earth Observing System (EOS) (AMSR-E) (Chelton and Wentz 2005), but also the surface meteorology from the ECMWF operational forecast analysis, ERA-40 (Uppala et al. 2005), and NCEP reanalyses (Kalnay et al. 1996; Kanamitsu et al. 2002). Consistent with the NWP model outputs, the synthesis produced U at 10 m, T_a and q_a at 2 m, and T_s at the sea surface. A height adjustment was applied to those input datasets that do not have the specified reference heights.

COADS ship observations were not a direct input data source in producing the daily synthesis from 1981 to 2005, but they, together with in situ buoy measurements, served as the base data to provide the estimates for error properties of each input dataset (Yu et al. 2004a). The error information determined the weights that prescribe the closeness of the least squares fitting between the analysis fields and input data fields. It should be noted that the NWP product fields are not completely independent of COADS, because many ship observations are assimilated by the NWP reanalysis models. The resulting synthesized fluxes were evaluated using more than 100 in situ measurement time series over the global oceans (Yu et al. 2004b). The in situ measurements included moored buoys at various locations acquired by the upper-ocean processes group at the Woods Hole Oceanographic Institution (Moyer and Weller 1997), the Pilot Research Moored Array in the Tropical Atlantic (PIRATA; Servain et al. 1998), and the Tropical Atmosphere Ocean (TAO) Triangle Trans-Ocean Buoy Network (TRITON) array in the tropical Pacific (McPhaden et al. 1998) and Indian (McPhaden et al. 2006) Oceans. Details of the evaluation analysis are presented in a separate document.

MEAN AND SEASONAL VARIABILITY. LHF and SHF increase with wind speed (U), near-surface vertical gradients of sea–air humidity ($\Delta q = q_s - q_a$), and temperature ($\Delta T = T_s - T_a$). Seasonally, the two fluxes are most significant in the extratropical regions in the fall and winter when the three variables, U, Δq, and ΔT, are at their maxima strength. Figure 2 shows the global distribution of LHF, SHF, and the sum of the two fluxes (LHF + SHF) in February and August, along with their respective annual means averaged over the 25-yr period from 1981 to 2005. Positive fluxes indicate heat loss from the ocean, while negative fluxes indicate heat gain by the ocean.

The seasonal variations in the Northern Hemisphere are largest over the two western boundary current (WBC) regions, that is, the Gulf Stream off of the United States, and the Kuroshio and its extension off of Japan. At these places, the maximum magnitude of LHF exceeds 300 W m^{-2} in February, but reduces to less than 100 W m^{-2} in August. Like the Northern Hemisphere, large seasonal changes in the Southern

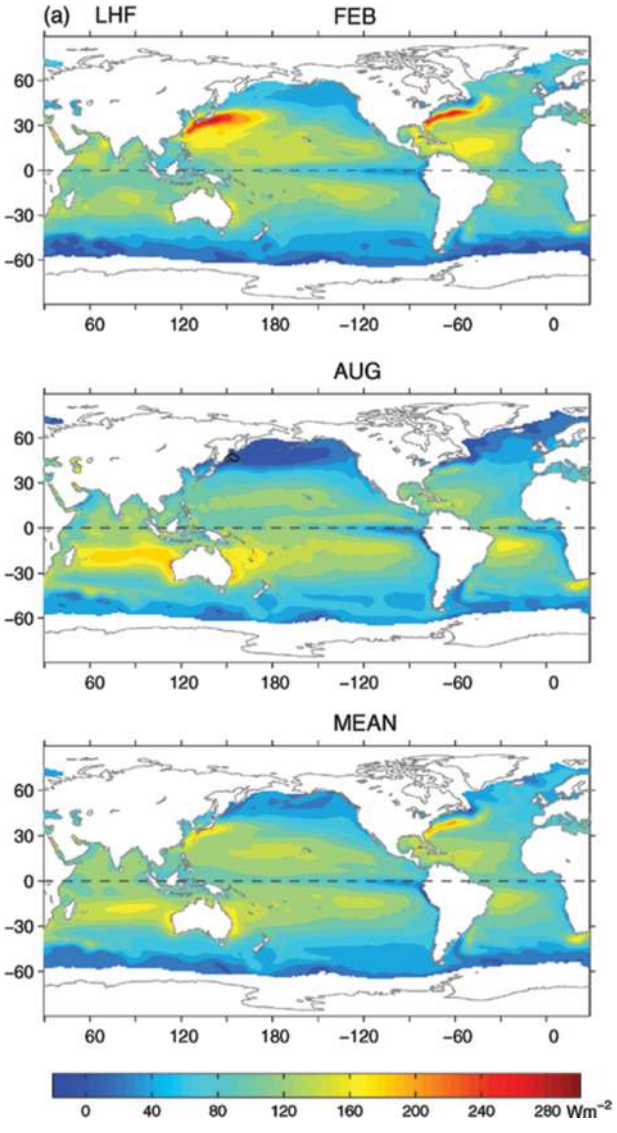

FIG. 2 (THIS PAGE AND NEXT). Surface (a) LHF, (b) SHF, and (c) LHF + SHF in February, August, and the annual mean (W m^{-2}). The fields represent the average over the 25-yr period from 1981 to 2005. Positive (negative) values denote upward (downward) fluxes. Zero contours are highlighted.

Hemisphere also occur over such boundary current regions as the Agulhas Current off the African coast, the Falkland–Brazilian Current off of South America, the Eastern Australian Current, and the Leeuwin Current off the west coast of Australia. Except for the last example, the other three are all western boundary currents. It is interesting to note that the flux intensification over these boundary current regions during the Southern Hemispheric wintertime is not as strong as their Northern Hemispheric counterparts. This is perhaps due to the fact that the continental landmasses of the Southern Ocean not only terminate in the subtropics, but also are relatively narrow, and so the air masses advected over the currents are less cold and dry.

The mean LHF and SHF over the global oceans have been extensively studied using either COADS or satellite observations (Esbensen and Kushnir 1981; Hsiung 1986; Oberhuber 1988; Cayan 1992a,b; da Silva et al. 1994; Chou et al. 1995; Schulz et al. 1997; Josey et al. 1999; Kubota et al. 2002; Bentamy et al. 2003; Grist and Josey 2003). Consistent with existing climatologies, the annual mean pattern of LHF reflects the dominant wintertime features of the two hemispheres. The largest LHF magnitudes (~200 W m^{-2}) are associated with the Gulf Stream and the Kuroshio and its extensions, while the second largest magnitudes (~150 W m^{-2}) are located over the broad subtropical southern Indian Ocean and the boundary regions associated with the Agulhas and the Eastern Australian Currents. LHF is relatively weak over the eastern Pacific and Atlantic cold tongues, and also at high northern and southern latitudes. Compared to LHF, SHF is generally weak. The magnitude of SHF over the open oceans is between –5 and 15 W m^{-2}, which is about one-tenth that of

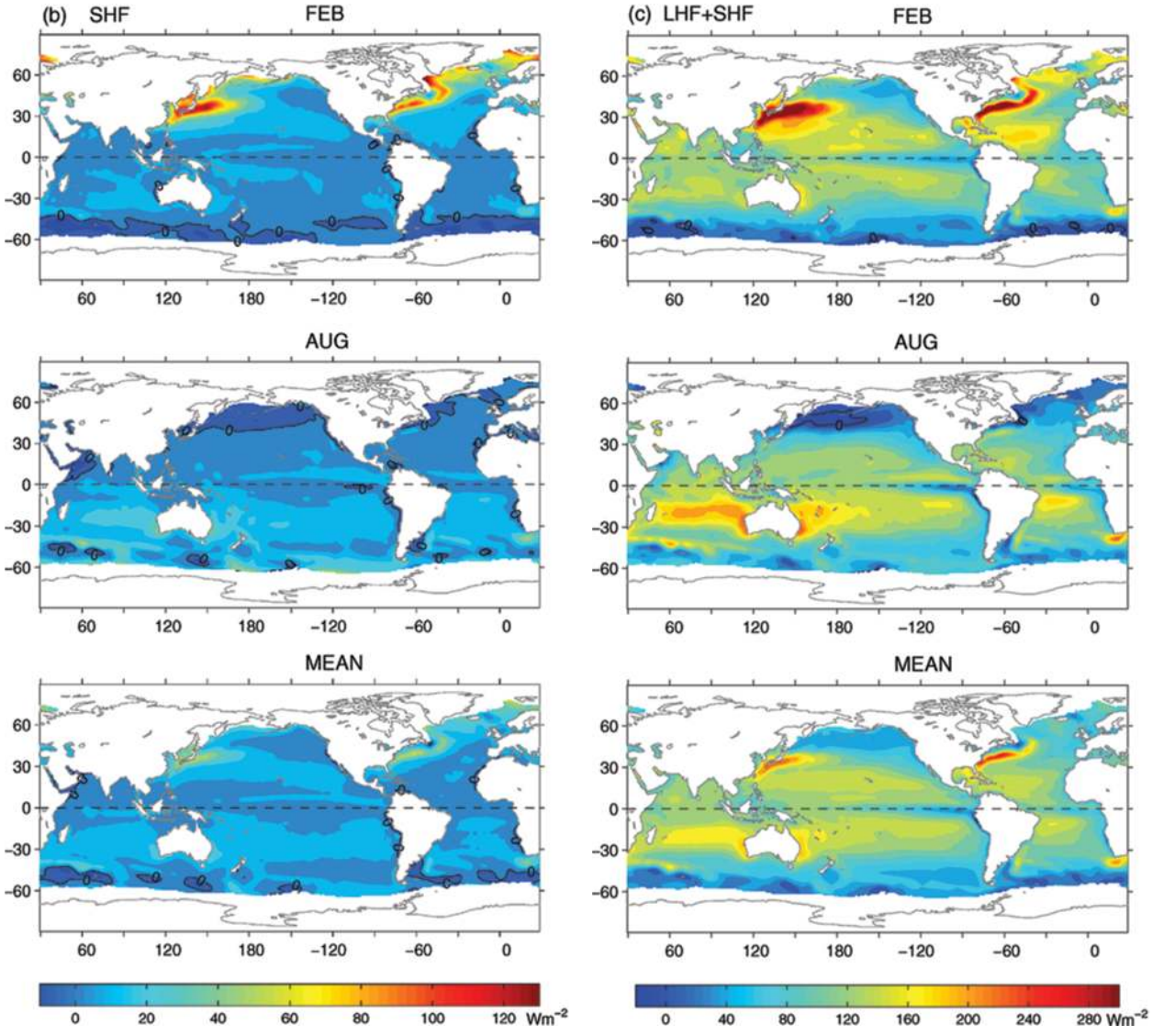

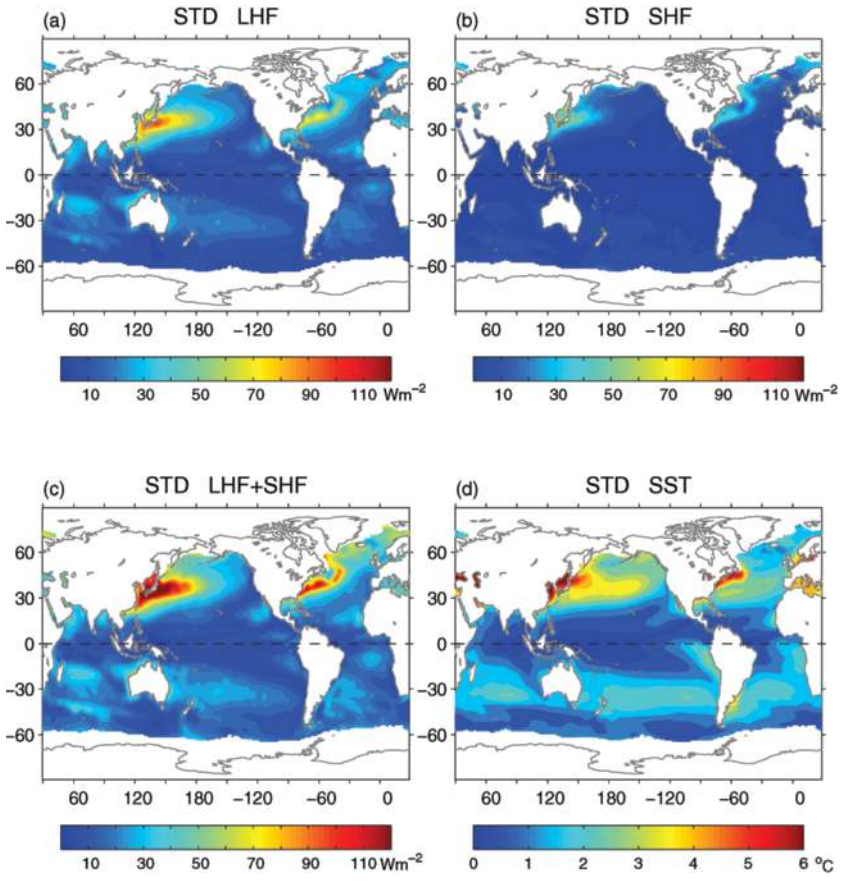

FIG. 3. STD of climatological monthly mean (a) LHF, (b) SHF, (c) LHF + SHF, and (d) SST with regard to the respective annual mean averaged over the period from 1981 to 2005.

LHF. SHF with a sufficient magnitude (>100 W m^{-2}) appears only in the boreal winter, in regions associated with the Kuroshio and Gulf Stream and its extensions and the northern North Atlantic (60°–80°N). LHF plus SHF accounts for the total turbulent oceanic heat loss to the atmosphere. Because SHF is small and its spatial distribution is similar to that of LHF, the pattern of LHF + SHF largely resembles the pattern of LHF, but with an enhanced magnitude.

To quantify the degree of the seasonal flux variability, the standard deviations (STD) of the climatological monthly means are computed for LHF, SHF, and LHF + SHF, respectively, using the following relation:

$$\sigma = \sqrt{\frac{\sum_{n=1}^{N}(x_n - \bar{x})^2}{N-1}}, \qquad (4)$$

where σ denotes the STD, and N is 12 (months); x represents the climatological (1981–2005) monthly mean fields of LHF, SHF, and LHF + SHF, while $\bar{x}$ is the annual mean field of the respective flux. As expected, the largest seasonal STDs in the three flux fields (Figs. 3a–c) are all located over the Gulf Stream, and the Kuroshio and its extensions. Interestingly, the magnitude and spatial extent of the variances associated with the Kuroshio system are greater than those with the Gulf Stream system, due largely to the fact that on seasonal time scales the air–sea fields of the former system have greater temporal and spatial variability. Figure 3d shows the STD of the seasonal SST variability as an example. The patterns of high/low variances in the fluxes are consistent with the patterns of the high/low variances of SST, suggesting an atmospheric response to oceanic forcing.

VARIABILITY ON INTERANNUAL AND LONGER TIME SCALES. By replacing x in (4) with the yearly averaged means for N = 25 yr 1981–2005) while retaining $\bar{x}$ as the long-term mean, the resulting yearly STD field measures the flux variability on interannual and longer time scales. The yearly STD maps for LHF, SHF, and LHF + SHF are shown in Figs. 4a–c. Compared to LHF, SHF yearly variability is generally small over the global basin except for the northern North Atlantic (i.e., the Labrador, Irminger, and Nordic Seas), where the variances of the two fluxes have a similar magnitude. There are also substantial SHF variances over the Gulf Stream and the Kuroshio regions, and the larger SHF variances associated with the former system appear to be induced primarily by the changes in air temperature.

The yearly STD fields have four features worth noting when compared to the seasonal STD patterns (Figs. 3a–c). First, and most strikingly, there are significant LHF variances in the equatorial Pacific and Indian Oceans, which is the region that features weak LHF variability on seasonal time scales. Second, the yearly variances of LHF and SHF are about an order of magnitude smaller than their seasonal counterparts.

Take LHF over the Kuroshio and its extensions as an example. The maximum yearly STD of LHF is less than 18 W m^{-2}, while the maximum seasonal STD exceeds 100 W m^{-2}. Third, the global boundary current regions, especially the Kuroshio and Gulf Stream and their extensions, are the location of primary variability for LHF on seasonal and interannual and longer time scales. Last, the high/low values of the yearly SST variances (Fig. 4d) do not always correspond to the high/low values of the yearly flux variances. This is particularly the case for the Indian Ocean.

Unlike the Indian Ocean, LHF and SST in the equatorial Pacific are closely related on time scales of El Niño–Southern Oscillation (Weare 1984; Zhang and McPhaden 1995; Wang and McPhaden 2001). The plots of the evolution of monthly LHF and SST anomalies averaged over the equatorial belt between 5°S and 5°N (Figs. 5a–b) show that the enhanced yearly LHF variances in the Pacific were indeed related to ENSO variability. In the central and eastern equatorial Pacific, positive LHF anomalies (increased latent heat loss) were associated with warm El Niño years, and negative LHF anomalies (reduced latent heat loss) with cold La Niña years. During the two great El Niño events in 1982/83 and 1997/98, a 4°C warming of the sea surface was accompanied by an increase of LHF by about 40 W m^{-2}.

ENSO also influences the atmosphere–ocean variability in the Indian and Atlantic Oceans. Nevertheless, the relationship between LHF and SST anomalies is rather different in the three equatorial oceans. The correlation coefficient between the two variables is 0.62 for the Pacific Ocean, 0.57 for the Atlantic Ocean, and 0.38 for the Indian Ocean. Although the coefficients are all significant at the 95% level, the degree of the correlation is less good in the equatorial Indian Ocean. This is seen in Figs. 5a–b. In the Atlantic Ocean, LHF and SST anomalies had a clear in-phase relationship throughout the 25-yr period, though the anomalies were much weaker compared to their Pacific counterparts. In the Indian Ocean, the two variables were out of phase in the 1980s, during which episodes of positive SST anomalies were associated with enhanced negative LHF anomalies. The correlation relationship was much improved in the late 1990s and early 2000s, because the two time series were both marked by coherent long-term upward trends. Similar upward trends in LHF and SST are also observed in the western equatorial Pacific.

LONG-TERM UPWARD TREND. The equatorial Indian and western Pacific Oceans constitute the so-called Indo-Pacific warm pool, that is, the location of maximum SSTs in the Tropics. It has been recognized that the SST in the Indo-Pacific warm pool has been rising in association with the global ocean warming (Cane et al. 1997). If so, has the long-term upward trend in LHF also occurred over a broad, global scale? To address the question, time series of yearly mean LHF, SHF, and LHF + SHF averaged over the global ice-free oceans are plotted (Figs. 6a–b). Clearly, the globally averaged LHF has been steadily

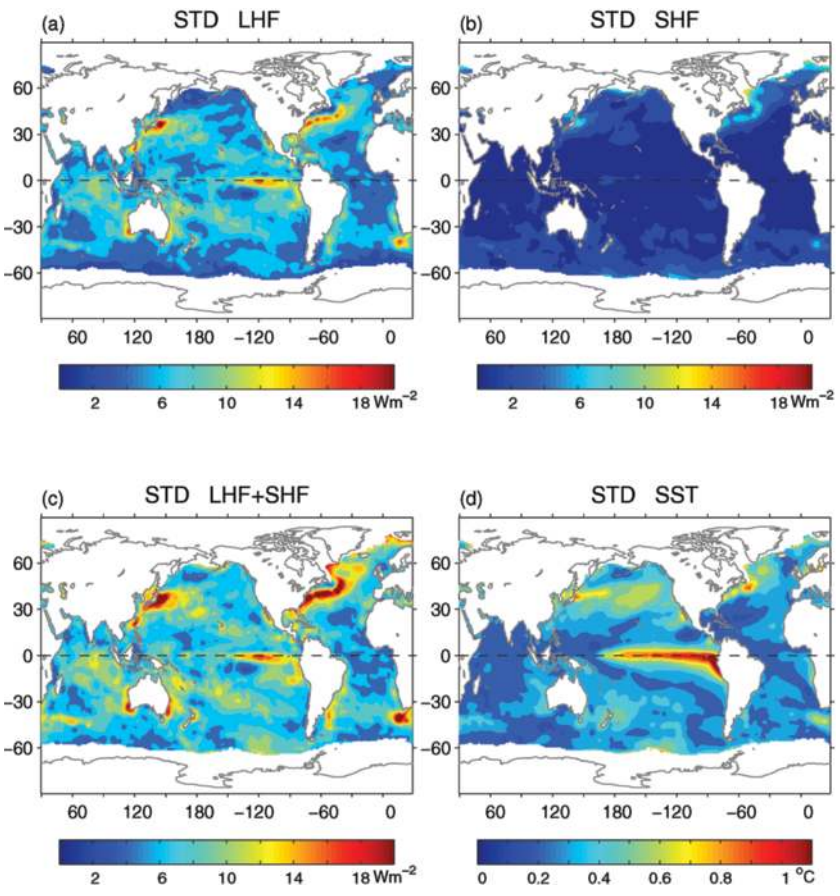

Fig. 4. STD of yearly mean (a) LHF, (b) SHF, (c) LHF + SHF, and (d) SST with regard to the respective long-term mean averaged over the period from 1981 to 2005.

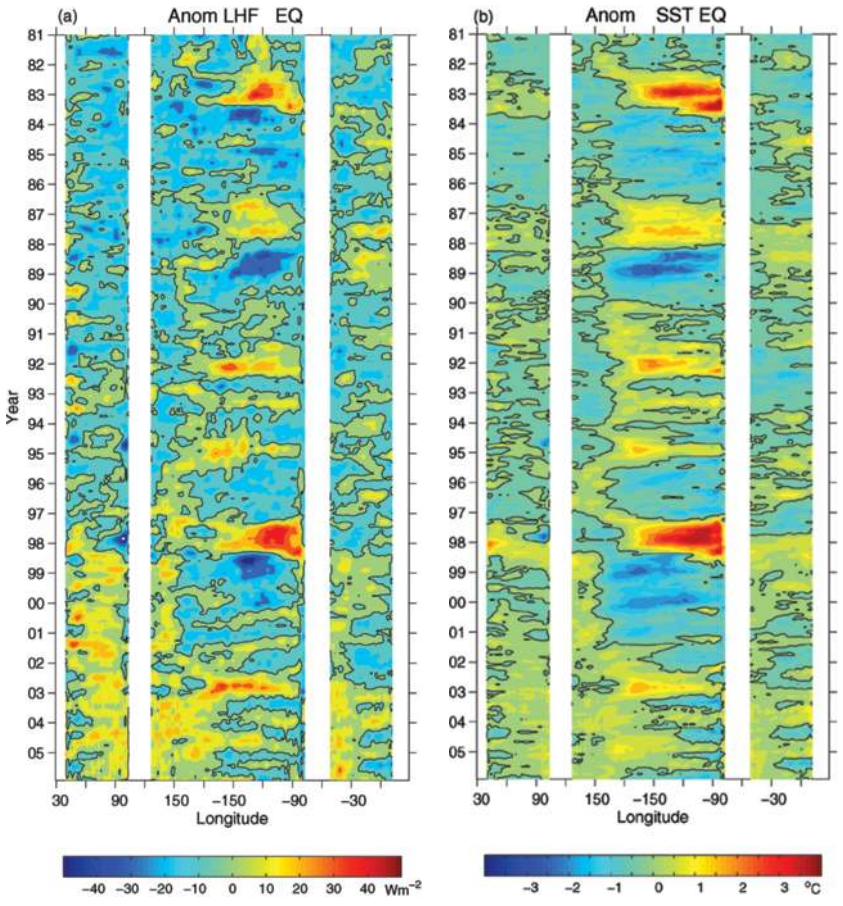

Fig. 5. Time–longitude plot of monthly mean anomalies of (a) LHF and (b) SST averaged in the equatorial band (5°S, 5°N). The mean seasonal cycle constructed over the period of 1981–2005 is subtracted. Zero contours are highlighted.

increasing since the beginning of the data record in 1981, with the increase being most pronounced in the 1990s. During this period, LHF has been up from the low at about 86 W m^{-2} in 1981 to the peak at about 95 W m^{-2} in 2002. There was a slight reduction in LHF after 2004, yet it is too early to tell whether this reduction was merely a perturbation of the long-term upward trend, as in the years of 1991 and 2001, or an indication of a change in the trend. By comparison, SHF shows no clear trend. A slight increase by about 1 W m^{-2} occurred in the 1990s followed by a quick reduction in the early 2000s. The mean SHF at the end of the data record in 2005 was back at a level similar to that in the early 1980s. In light of the small change in SHF, the near-linear increase in the globally averaged LHF + SHF reflects the trend in LHF.

SST over the global oceans has been rising since the late nineteenth century (Cane et al. 1997), with the most rapid warming occurring in the decades of the 1980s and 1990s (Cane et al. 1997; Lau and Weng 1999). Time series of yearly mean SST averaged over the global ice-free oceans produced by OAFlux indicates an increase in SST by about 0.3°C since 1981 (Fig. 6c). Unlike the LHF time series that shows a quasi-linear trend, the SST record is marked by large interannual fluctuations related to ENSO superimposed on a slowly warming trend. Nevertheless, Figs. 6a–c suggest that the increase of the global LHF is a response to the global SST.

To explore the cause of the long-term increase in LHF, linear trends for both LHF and the flux-related variables (i.e., SST, sea–air humidity difference Δq, air humidity q_a, and wind speed U) were derived using the yearly mean fields over the entire data record (1981–2005) (Figs. 7a–e). The upward trends in LHF had a large-scale structure that is significant in the equatorial Indo-Pacific warm pools and along the ITCZ; the latter is displaced just north of the equator in the Pacific and Atlantic Oceans. Outside of the tropical oceans, pronounced upward trends occurred over the global boundary current regions, including the Kuroshio and its extension, the Gulf Stream and its extension, the Agulhas Current, the Falkland–Brazil Currents, the Eastern Australian Current, and the Leeuwin Current. Despite the overall positive trends, weak negative trends existed in subtropical regions such as the eastern Pacific and Atlantic Oceans and the western southern Indian Ocean.

Positive LHF trends are well correlated with positive SST trends (Fig. 7b), while negative LHF trends are correlated with negative and/or weak positive SST trends. The signs of the LHF trends have an overall consistency with the signs of the SST trends over most global basins, with the exception of the North Atlantic Ocean. In the latter case, a rising SST is featured over the entire domain with the maximum warming rate in the northern North Atlantic. Despite the large increase in SST, LHF shows only weak positive trends in the northern basin and negative trends in the subtropical Atlantic.

The sea–air humidity difference Δq is a function of SST. Figure 7c shows that Δq was the key variable connecting the trend patterns between LHF and SST. The regions of positive (negative) LHF trends were largely predefined by the regions of positive (negative) Δq trends. The determination of Δq by SST is due to the fact that SST not only determines the sea surface saturation specific humidity (q_s), but also modulates the large-scale structure of the near-surface air humidity (q_a). It is not a surprise to see (Fig. 7d) that there is a SST influence in the linear trend pattern of q_a, and it showed downward trends in the eastern Pacific and at high southern latitudes with upward trends elsewhere.

The trends in wind speed U (Fig. 7e) are predominantly upward, being most coherent in the south oceans and the tropical Indian Ocean. Slight negative trends are observed in the tropical and central North Pacific and the tropical Atlantic. Unlike Δq, the trend pattern of U is less correlated with that of LHF, suggestive of a nonlocal relationship between U and LHF. It is worth noting that the roles of U and Δq in LHF are fundamentally different. A nonzero Δq, not U, is a prerequisite for latent evaporation to occur; U facilitates the evaporation by carrying water vapor away from the evaporating sea surface and helps to reestablish Δq at a faster pace. In other words, the magnitude of U modulates the effect of Δq on LHF, and a stronger U promotes larger LHF. It is further worth noting that the relationship between U and SST is not necessarily local, because the large-scale pattern of U is influenced by SST gradients rather than SST itself. This explains why the trend pattern of U is not locally correlated with either SST or LHF.

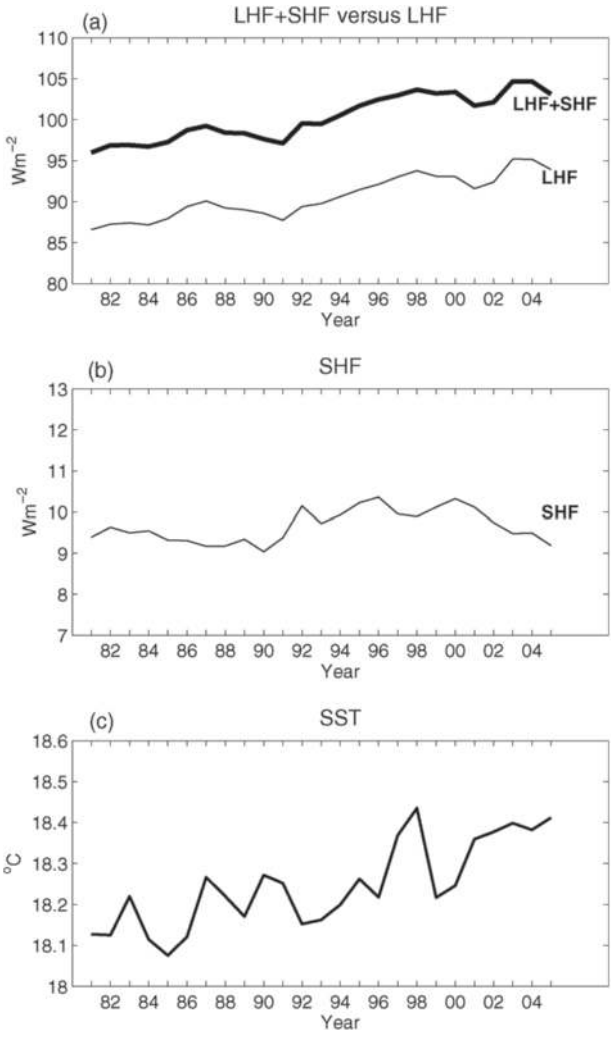

Fig. 6. Year-to-year variations of yearly mean (a) LHF versus LHF + SHF, (b) SHF, and (c) SST averaged over the global ice-free oceans.

SUMMARY AND DISCUSSION. Daily LHF and SHF estimates over the global ice-free oceans from 1981 to 2005 have been produced by the Objectively Analyzed Air–Sea Fluxes (OAFlux) project through synthesizing surface meteorology obtained from satellite remote sensing and NCEP and ECMWF numerical weather prediction model reanalyses. The methodology and technique were built upon an initial study of the Atlantic Ocean that demonstrated that such data synthesis improves daily flux estimates over the basin scale (Yu et al. 2004a,b, 2006). The OAFlux project has an objective of producing an enhanced global air–sea heat flux analysis from the mid-1950s to the present. The 25-yr time series of latent heat flux (LHF) and sensible heat flux (SHF) presented here were the first outcome of the project.

This paper used the new global flux dataset to analyze, understand, and document the patterns and variability of the LHF and SHF fields on annual, seasonal, interannual, and decadal time scales. It is found that, among all of the climate signals investigated, the most striking is a long-term increase in LHF that dominates the 25-yr data record. The globally averaged latent heat flux has increased by roughly 9 W m^{-2} between the low in 1981 and the peak in 2002, which amounts to about a 10% increase in the mean value over the 25-yr period. Positive linear trends appeared on a global scale, with the most significant in the tropical Indian and western Pacific warm pools and the boundary current regions.

The period of 1981–2005 covered by the dataset was marked by the warming of the global oceans at a fast pace (Levitus et al. 2005). The trend pattern of LHF bears a great similarity to that of SST, suggestive of an atmospheric response to oceanic forcing. The analysis of the linear trends in flux-related variable

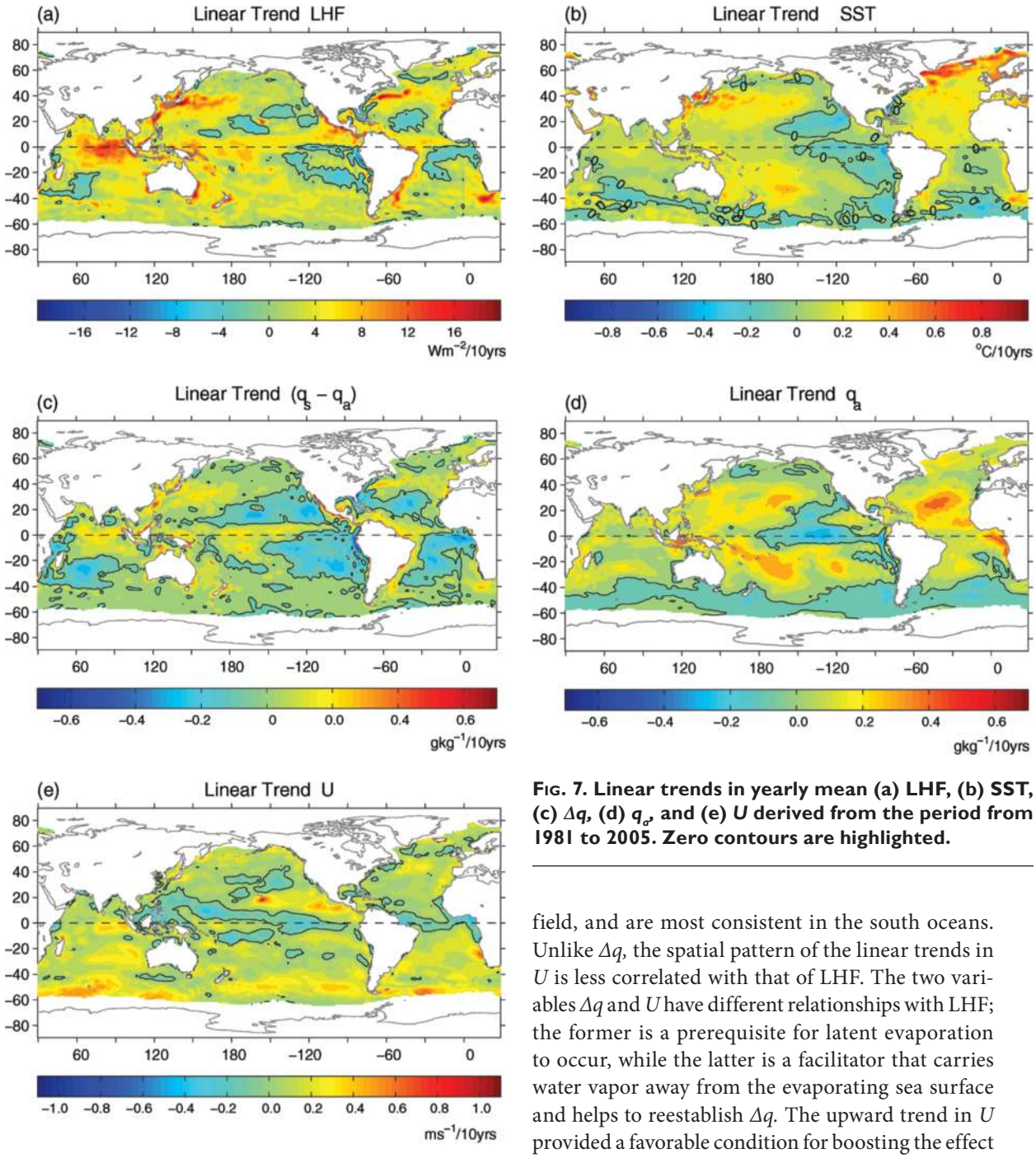

FIG. 7. Linear trends in yearly mean (a) LHF, (b) SST, (c) Δq, (d) q_a, and (e) U derived from the period from 1981 to 2005. Zero contours are highlighted.

fields [e.g., air humidity (q_a), sea–air humidity differences (Δq), and wind speed (U)] showed that Δq was the link between SST and LHF. Regions of positive (negative) trends of Δq define the regions of positive (negative) trends in LHF. SST affects Δq, because SST not only determines q_s but also modulates the large-scale structure of q_a. Hence, the moisture-holding capacity of the atmosphere goes up as a result of global warming, and this further promotes latent evaporation. Positive trends are also shown in the global U field, and are most consistent in the south oceans. Unlike Δq, the spatial pattern of the linear trends in U is less correlated with that of LHF. The two variables Δq and U have different relationships with LHF; the former is a prerequisite for latent evaporation to occur, while the latter is a facilitator that carries water vapor away from the evaporating sea surface and helps to reestablish Δq. The upward trend in U provided a favorable condition for boosting the effect of Δq and allowing a continued increase of LHF.

An enhanced oceanic latent heat loss under global warming is anticipated from the viewpoint of the Clausius–Clapeyron equation. However, it should be noted that the estimated change in LHF found in this study, which is about 10 W m^{-2} over the 1981–2005 period, appears to be an order of magnitude larger than the value of 1 W m^{-2} given by the recent climate model analyses of Pierce et al. (2006). The latter study represents the model simulation of the response of the climate system to global warming. The large difference

between our data-based estimation and the model analyses of Pierce et al. suggests the need to reconcile the differences between the flux analyses and climate models. The major uncertainty in our analysis is the near-surface air humidity due to the lack of direct observations. Nevertheless, the total 10 W m^{-2} increase is roughly equal between Δq and U. The wind fields are supposed to be a better-measured quantity, especially since SSM/I became available later in 1987.

The relationship between LHF and SST was emphasized in the study because the two variables are related but not the same. LHF contains richer information than SST. LHF is the function of near–sea surface circulation, humidity, and temperature, and thus is not dependent solely upon SST. Moreover, the atmosphere interacts with the ocean through air–sea fluxes, not SST, though SST is a key variable that affects air–sea heat exchange processes. The study showed that on seasonal time scales the oceanic heat fluxes are the response to the SST forcing. On interannual and longer time scales, the influence of ENSO SST on LHF in the eastern equatorial Pacific is clearly shown; elsewhere the correlation between the two variables is not always as good. Major differences occurred in the tropical Indian and western Pacific Oceans, where there were sufficient year-to-year variances in LHF but not in SST.

This paper provided data-based evidence of an increase of sea–air humidity differences, and hence LHF, under global warming; it also suggested that the increase in wind speed is the other contributor to the change in LHF. Latent heat exchange at the air–sea interface results in the transport of both energy and water vapor into the atmosphere. The enhanced latent heat evaporation in the past 25 yr would lead to an increased transport of water vapor into the atmosphere. This is supported by observational evidence that the upward trends in the moisture content in the lower troposphere are averaging 1.3 ± 0.3% $decade^{-1}$ during 1988–2003 for the ocean as a whole (Trenberth et al. 2005). There are three potential consequences as a result of enhanced latent heat evaporation. First, water vapor is a key element of the hydrological cycle, that is, the cycling of water, in all three phases, within and between the Earth's atmosphere, oceans, and continents. The movement of water vapor in the hydrological cycle is coupled with precipitation and soil moisture. Does the enhanced oceanic evaporation imply an increased hydrological cycle? Second, water vapor is an important greenhouse gas. As the temperature of the Earth's surface and atmosphere increases, the atmosphere is able to hold more water vapor (Held and Soden 2000). The additional water vapor, acting as a greenhouse gas, absorbs and reemits the infrared radiation back to the Earth's surface, and so causes further warming. How much of the change in longwave radiation is attributed to the increased water vapor? Last, the salinity in the ocean mixed layer would increase due to the loss of water vapor to the atmosphere. The salinification impacts not only the thermohaline circulation, which is strongly influenced by the surface salinity differences between the subpolar and the subtropical oceans, but also the mixed layer structure that, in turn, influences the way that the ocean and the atmosphere interact.

The air–sea fluxes to and from the ocean force the atmospheric circulation and, at the same time, control the ocean temperature. We anticipate that this new flux product will help to improve the understanding of not only the variability of air–sea heat fluxes and their role in weather and climate, but also the role of the world's oceans in the coupled ocean–atmosphere system.

ACKNOWLEDGMENTS. The authors gratefully acknowledge support from NOAA through the Cooperative Institute for Climate and Oceanic Research (CICOR) at the Woods Hole Oceanographic Institution (WHOI). Supporting NOAA grants are from the Office of Climate Observations (OCO) and Climate Change Data and Detection (CCDD). Xiangze Jin provided programming and analysis support and Kelan Huang processed ECMWF datasets. Satellite wind and temperature products are downloaded from the Remote Sensing Systems Company (www.ssmi.com) and the JPL Physical Oceanography Distributed Active Archive Center (PODAAC; online at http://podaac-www.jpl.nasa.gov/), and NCEP and ECMWF reanalyses outputs are from the Data Support Section at NCAR.

REFERENCES

Atlas, R., R. Hoffman, S. Bloom, J. Jusem, and J. Ardizzone, 1996: A multi-year global surface wind velocity dataset using SSM/I wind observations. *Bull. Amer. Meteor. Soc.,* **77,** 869–882.

Bergthorsson, P., and B. Döös, 1955: Numerical weather map analysis. *Tellus,* **7,** 329–340.

Betamy, A., K. B. Katsaros, A. M. Mestas-Nuñez, W. M. Drennan, E. B. Forde, and H. Roquet, 2003: Satellite estimates of wind speed and latent heat flux over the global oceans. *J. Climate,* **16,** 637–656.

Bunker, A. F., 1976: Computations of surface energy flux and annual air-sea interaction cycles of the North Atlantic Ocean. *Mon. Wea. Rev.,* **104,** 1122–1140.

——, 1980: Trends of variables and energy fluxes over the Atlantic Ocean from 1948 to 1972. *Mon. Wea. Rev.,* **108,** 720–732.

Cane, M. A., A. C. Clement, A. Kaplan, Y. Kushnir, D. Pozdnyakov, R. Seager, S. E. Zebiak, and R. Murtugudde, 1997: Twentieth-century sea surface temperature. *Science,* **275,** 957–960.

Cayan, D. R., 1992a: Latent and sensible heat flux anomalies over the Northern Oceans: The connection to monthly atmospheric circulation. *J. Climate,* **5,** 354–369.

——, 1992b: Latent and sensible heat flux anomalies over the Northern Oceans: Driving the sea surface temperature. *J. Phys. Oceanogr.,* **22,** 859–881.

Chelton, D. B., and F. J. Wentz, 2005: Global microwave satellite observations of sea surface temperature for numerical weather prediction and climate research. *Bull. Amer. Meteor. Soc.,* **86,** 1097–1115.

Chou, S.-H., R. Atlas, C.-L. Shie, and J. Ardizzone, 1995: Estimates of surface humidity and latent heat fluxes over oceans from SSMI data. *Mon. Wea. Rev.,* **123,** 2405–2425.

——, E. Nelkin, J. Ardizzone, R. M. Atlas, and C.-L. Shie, 2003: Surface turbulent heat and momentum fluxes over global oceans based on the Goddard satellite retrievals, version 2 (GSSTF2). *J. Climate,* **16,** 3256–3273.

Curry, J. A., C. A. Clayson, W. B. Rossow, R. Reeder, Y. C. Zhang, P. J. Webster, G. Liu, and R. S. Sheu, 1999: High-resolution satellite-derived dataset of the ocean surface fluxes of heat, freshwater and momentum for the TOGA COARE IOP. *Bull. Amer. Meteor. Soc.,* **80,** 2059–2080.

Daley, R., 1991: *Atmospheric Data Analysis.* Cambridge University Press, 457 pp.

da Silva, A. M., C. C. Young, and S. Levitus, 1994: *Anomalies of Heat and Momentum Fluxes.* Vol. 3, *Atlas of Surface Marine Data,* NOAA Atlas NESDIS 8, 413 pp.

Esbensen, S. K., and V. Kushnir, 1981: The heat budget of the global oceans: An atlas based on estimates from marine surface observations. Oregon State University Climate Research Institute Rep. 29, 271 pp.

Fairall, C. W., E. F. Bradley, D. P. Rogers, J. B. Edson, and G. S. Young, 1996: Bulk parameterization of air-sea fluxes for Tropical Ocean–Global Atmosphere Coupled–Ocean Atmosphere Response Experiment. *J. Geophys. Res.,* **101** (C2)**,** 3747–3764.

——, ——, J. E. Hare, A. A. Grachev, and J. B. Edson, 2003: Bulk parameterization of air-sea fluxes: Updates and verificaiton for the COARE algorithm. *J. Climate,* **16,** 571–591.

Grist, J. P., and S. A. Josey, 2003: Inverse analysis adjustment of the SOC air–sea flux climatology using ocean heat transport constraints. *J. Climate,* **16,** 3274–3295.

Held, I. M., and B. J. Soden, 2000: Water vapor feedback and global warming. *Ann. Rev. Energy Environ.,* **25,** 441–475.

Hsiung, J., 1985: Estimates of global oceanic meridional heat transport. *J. Phys. Oceanogr.,* **15,** 1405–1413.

Isemer, H.-J., and L. Hasse, 1985: *The Bunker Climate Atlas of the North Atlantic Ocean: 1. Observations.* Springer-Verlag, 218 pp.

——, and ——, 1987: *The Bunker Climate Atlas of the North Atlantic Ocean: 2. Air–Sea Interactions.* Springer-Verlag, 256 pp.

Josey, S. A., 2001: A comparison of ECMWF and NCEP/NCAR surface heat fluxes with moored buoy measurements in the subduction region of the northeast Atlantic. *J. Climate,* **14,** 1780–1789.

——, E. C. Kent, and P. K. Taylor, 1998: *The Southampton Oceanography Centre (SOC) Ocean–Atmosphere Heat, Momentum and Freshwater Flux Atlas.* Southampton Oceanography Centre Rep. 6, 30 pp + figures.

——, ——, and ——, 1999: New insights into the ocean heat budget closure problem from analysis of the SOC air–sea flux climatology. *J. Climate,* **12,** 2850–2880.

Kalnay, E., and Coauthors, 1996: The NCEP/NCAR 40-Year Reanalysis Project. *Bull. Amer. Meteor. Soc.,* **77,** 437–471.

Kanamitsu, M., W. Ebisuzaki, J. Woolen, J. Potter, S-K Yang, J.J. Hnilo, M. Fiorino, and G. L. Potter, 2002: NCEP-DEO AMIP-II Reanalysis (R-2). *Bull. Atmos. Met. Soc.,* **83,** 1631–1643.

Kubota, M., N. Iwasaka, S. Kizu, M. Konda, and K. Kutsuwada, 2002: Japanese Ocean Flux data dets with Use of Remote sensing Observations (J-OFURO). *J. Oceanogr.,* **58,** 213–225.

Legler, D. M., I. M. Navon, and J. J. O'Brien, 1989: Objective analysis of pseudostress over the Indian Ocean using a direct-minimization approach. *Mon. Wea. Rev.,* **117,** 709–720.

Levitus, S., J. I. Antonov, T. P. Boyer, and C. Stephens, 2000: Warming of the world ocean. *Science,* **287,** 2225–2229.

——, ——, and ——, 2005: Warming of the world ocean, 1955–2003. *Geophys. Res. Lett.,* **32,** L02604, doi:10.1029/2004GL021592.

Liu, W. T., 1988: Moisture and latent heat fluxes: Variabilities in the tropical Pacific derived from satellite data. *J. Geophys. Res.,* **93,** 6749–6769.

——, K. B. Katsaros, and J. A. Businger, 1979: Bulk parameterization of air–sea exchanges of heat and water vapor including the molecular constraints at the interface. *J. Atmos. Sci.,* **36,** 1722–1735.

McPhadden, M. J., and Coauthors, 1998: The Tropical Ocean-Global Atmosphere (TOGA) observing

system: A decade of progress. *J. Geophys. Res.,* **103,** 14 169–14 240.

——, Y. Kuroda, and V. S. N. Murty, 2006: Development of an Indian Ocean moored buoy array for climate studies. *CLIVAR Exchanges,* International CLIVAR Office, Southampton, United Kingdom, Vol. 11, No. 4, 3–5.

Moyer, K. A., and R. A. Weller, 1997: Observations of surface forcing from the Subduction Experiment: A comparison with global model products and climatological datasets. *J. Climate,* **10,** 2725–2742.

Niiler, P. P., and E. B. Kraus, 1977: One-dimensional models of the upper ocean. *Modelling and Prediction of the Upper Layers of the Ocean,* E. B. Kraus, Ed., Pergamon, 143–172.

Oberhuber, J. M., 1988: An atlas based on COADS data set: The budget of heat, buoyancy and turbulent kinetic energy at the surface of the Global Ocean. MPI Rep. 15, 1999 pp.

Panofsky, H. A., 1949: Objective weather map analysis. *J. Meteor.,* **6,** 386–392.

Pierce, D. W., T. P. Barnett, K. M. Achutarao, P. J. Gleckler, J. M. Gregory, and W. M. Washington, 2006: Anthropogenic warming of the oceans: Observations and model results. *J. Climate,* **19,** 1873–1900.

Reynolds, R. W., N. A. Rayner, T. M. Smith, D. C. Stokes, and W. Wang, 2002: An improved in situ and satellite SST analysis for climate. *J. Climate,* **15,** 1609–1625.

Schulz, J., P. Schlüssel, and H. Graβl, 1993: Water vapor in the atmospheric boundary layer over oceans from SSM/I measurements. *Int. J. Remote Sens.,* **14,** 2773–2789.

——, J. Meywerk, S. Ewald, and P. Schlussel, 1997: Evaluation of satellite-derived latent heat fluxes. *J. Climate,* **10,** 2782–2795.

Servain, J., A. J. Busalacchi, M. J. McPhaden, A. D. Moura, G. Reverdin, M. Vianna, and S. E. Zebiak, 1998: A Pilot Research Moored Array in the Tropical Atlantic (PIRATA). *Bull. Amer. Meteor. Soc.,* **79,** 2019–2031.

Simonot, J.-Y. R., and C. Gautier, 1989: Satellite estimates of surface evaporation in the Indian Ocean during the 1979 monsoon. *Ocean-Air Inter.,* **1,** 239–256.

Smith, S. R., D. M. Legler, and K. V. Verzone, 2001: Quantifying uncertainties in NCEP reanalyses using high-quality research vessel observations. *J. Climate,* **14,** 4062–4072.

Trenberth, K. E., J. Fasullo, and L. Smith, 2005: Trends and variability in column-integrated atmospheric water vapor. *Climate Dyn.,* **24,** 741–758.

Uppala, S., and Coauthors, 2005: The ERA-40 re-analysis. *Quart. J. Roy. Meteor. Soc.,* **131,** 2961–3012.

Wang, W., and M. J. McPhaden, 2001: Surface layer heat balance in the equatorial Pacific Ocean during the 1997–98 El Niño and the 1998–99 La Niña. *J. Climate,* **14,** 3393–3407.

Weare, B. C., 1984: Interannual moisture variations near the surface of the tropical Pacific Ocean. *Quart. J. Roy. Meteor. Soc.,* **110,** 489–504.

Weller, R. A., M. F. Baumgartner, A. S. Josey, A. S. Fischer, and J. Kindle, 1998: Atmospheric forcing in the Arabian Sea during 1994–1995: Observations and comparisons with climatology and models. *Deep Sea. Rev.,* **45,** 1961–1999.

Wentz, F. J., 1997: A well-calibrated ocean algorithm for SSM/I. *J. Geophys. Res.,* **102,** 8703–8718.

WGASF, 2000: Intercomparison and validation of ocean–atmosphere energy flux fields. WCRP/SCOR Working Group on Air–Sea Fluxes Series Rep. 112, WMO/TD 1036, 303 pp.

Woodruff, S. D., H. F. Diaz, J. D. Elms, and S. J. Worley, 1998: COADS Release 2 data and metadata enhancements for improvements of marine surface flux fields. *Phys. Chem. Earth,* **23,** 517–526.

Xie, P., and P. A. Arkin, 1996: Analyses of global monthly precipitation using gauge observations, satellite estimates and numerical model predictions. *J. Climate,* **9,** 840–858.

Yu, L., R. A. Weller, and B. Sun, 2004a: Improving latent and sensible heat flux estimates for the Atlantic Ocean (1988–1999) by a synthesis approach. *J. Climate,* **17,** 373–393.

——, ——, and ——, 2004b: Mean and variability of the WHOI daily latent and sensible heat fluxes at in situ flux measurement sites in the Atlantic Ocean. *J. Climate,* **17,** 2096–2118.

——, X. Jin, and R. A. Weller, 2007: Annual, seasonal, and interannual variability of air–sea heat fluxes in the Indian Ocean. *J. Climate,* in press.

——, ——, and ——, 2006: Role of net surface heat flux in seasonal variations of sea surface temperature in the tropical Atlantic Ocean. *J. Climate,* **19,** 6153–6169.

Zhang, G.-J., and M. J. McPhaden, 1995: The relationship between sea surface temperature and latent heat flux in the equatorial Pacific. *J. Climate,* **8,** 589–605.

Zhang, Y.-C., W. B. Rossow, A. A. Lacis, V. Oinas, and M. I. Mishchenko, 2004: Calculation of radiative fluxes from the surface to top of atmosphere based on ISCCP and other global data sets: Refinements of the radiative transfer model and the input data. *J. Geophys. Res.,* **109,** D19105, doi:10.1029/2003JD004457.